Development of a novel fluorogenic proteolytic beacon for *in vivo* detection and imaging of tumour-associated matrix metalloproteinase-7 activity

J. Oliver McINTYRE*[1], Barbara FINGLETON*, K. Sam WELLS†, David W. PISTON†, Conor C. LYNCH*, Shiva GAUTAM‡[2] and Lynn M. MATRISIAN*

*Department of Cancer Biology, Vanderbilt University School of Medicine, Nashville, TN 37232-6840, U.S.A., †Departments of Molecular Physiology and Biophysics, Vanderbilt University School of Medicine, Nashville, TN 37232-6840, U.S.A., and ‡Department of Preventative Medicine, Vanderbilt University School of Medicine, Nashville, TN 37232-6840, U.S.A.

The present study describes the *in vivo* detection and imaging of tumour-associated MMP-7 (matrix metalloproteinase-7 or matrilysin) activity using a novel polymer-based fluorogenic substrate PB-M7VIS, which serves as a selective 'proteolytic beacon' (PB) for this metalloproteinase. PB-M7VIS is built on a PAMAM (polyamido amino) dendrimer core of 14.2 kDa, covalently coupled with an Fl (fluorescein)-labelled peptide Fl(AHX)RPLALWRS(AHX)C (where AHX stands for aminohexanoic acid) and with TMR (tetramethylrhodamine). PB-M7VIS is efficiently and selectively cleaved by MMP-7 with a k_{cat}/K_m value of 1.9×10^5 $M^{-1} \cdot s^{-1}$ as measured by the rate of increase in Fl fluorescence (up to 17-fold for the cleavage of an optimized PB-M7VIS) with minimal change in the TMR fluorescence. The K_m value for PB-M7VIS is approx. 0.5 μM, which is approx. two orders of magnitude lower when compared with that for an analogous soluble peptide, indicating efficient interaction of MMP-7 with the synthetic polymeric substrate. With MMP-2 or -3, the k_{cat}/K_m value for PB-M7VIS is approx. 56- or 13-fold lower respectively, when compared with MMP-7. In PB-M7VIS, Fl(AHX)RPLALWRS(AHX)C is a selective optical sensor of MMP-7 activity and TMR serves to detect both the uncleaved and cleaved reagents. Each of these can be visualized as subcutaneous fluorescent phantoms in a mouse and optically discriminated based on the ratio of green/red (Fl/TMR) fluorescence. The *in vivo* specificity of PB-M7VIS was tested in a mouse xenograft model. Intravenous administration of PB-M7VIS gave significantly enhanced Fl fluorescence from MMP-7-positive tumours, but not from control tumours ($P < 0.0001$), both originally derived from SW480 human colon cancer cells. Prior systemic treatment of the tumour-bearing mice with an MMP inhibitor BB-94 {[4-(*N*-hydroxyamino)-2*R*-isobutyl-3*S*-(thienylthiomethyl)-succinyl]-L-phenylalanine-*N*-methylamide}, markedly decreased the Fl fluorescence over the MMP-7-positive tumour by approx. 60 %. Thus PB-M7VIS functions as a PB for *in vivo* detection of MMP-7 activity that serves to light this optical beacon and is, therefore, a selective *in vivo* optical molecular imaging contrast reagent.

Key words: fluorescence assay, fluorogenic dendrimer, matrix metalloproteinase-7 (MMP-7), optical molecular imaging, proteolytic beacon, SW480 xenograft.

INTRODUCTION

MMPs (matrix metalloproteinases) are a family of extracellular, zinc-dependent proteinases that are capable of degrading all components of the extracellular matrix (see [1,2] for reviews). Of the 23 identified human MMP gene products, MMP-7 is distinct in a number of characteristics (see [3] for a review). It is notable that MMP-7 is produced predominantly by cells of epithelial origin, whereas most MMPs are generally expressed by the underlying stromal cells including those residing in connective tissues or by migratory cells of the immune system. In addition, MMP-7 is one of the few MMPs whose expression can be detected in benign intestinal tumours [4]. MMP-7 has been shown to be important in the progression of a number of tumours, notably those originating in the colon or in the breast. Studies in mice [5,6] indicate that MMP-7 may serve as a suitable target for controlling disease progression in patients with high risk for colon cancer. From a functional imaging perspective, MMP-7 provides a focused source of an abundantly expressed extracellular enzyme, properties that are anticipated to facilitate its *in vivo* detection and quantitative analysis. Thus MMP-7 presents an excellent target for the development of a 'proteolytic beacon' (PB) designed for the *in vivo* detection of metalloproteinase activity.

Non-invasive imaging techniques provide an approach to detect specific molecular events *in vivo* from which therapeutic strategies might be devised and tested. Previous studies have demonstrated the potential for these strategies, including the application of fluorescent probes to detect and measure both proteolytic activity and its inhibition *in vivo* [7–9]. In particular, near-IR fluorescent reagents with different peptide sequences have been used to detect either cathepsin B [8] or MMP-2 [9] activities in tumours. With the latter reagent, the treatment of tumour-bearing mice with prinomastat, an MMP-2/9-selective MMPI (MMP inhibitor), significantly decreased tumour-associated enzyme activity as measured by near-IR fluorescent optical imaging.

A variety of fluorogenic protein reagents have been described, including fluorescence-labelled collagens and gelatin that can serve as substrates for proteases including MMPs. In addition, there are a number of more selective fluorogenic peptide substrates for proteases, including some that can be cleaved by MMPs. One such fluorogenic peptide was designed for cleavage by MMP-7 [10]. These kinds of peptide-based substrates serve to assay

Abbreviations used: AHX, aminohexanoic acid; BB-94, [4-(*N*-hydroxyamino)-2*R*-isobutyl-3*S*-(thienylthiomethyl)-succinyl]-L-phenylalanine-*N*-methylamide; DQ, dye-quenched; Fl, fluorescein; MMP, matrix metalloproteinase; MMPI, MMP inhibitor; MRI, magnetic resonance imaging; PAMAM, polyamido amino; PB, proteolytic beacon; SIA, *N*-succinimidyl iodoacetate; TMR, tetramethylrhodamine; TRITC, TMR β-isothiocyanate; WSR, Wilcoxon Sign Rank.

[1] To whom correspondence should be addressed (e-mail oliver.mcintyre@vanderbilt.edu).

[2] Present address: Beth Israel Deaconess Medical Center and Harvard Medical School, Boston, MA, U.S.A.

MMP activities *in vitro*, but have not been used as *in vivo* reporters of enzymic activity. In the present study, we describe the design and synthesis of a novel polymer-based fluorogenic substrate PB-M7VIS, which can be selectively cleaved by MMP-7. This fluorogenic substrate is built on a dendrimeric PAMAM (polyamido amino) scaffold, which has been shown previously to have tolerance to rodents after *in vivo* injection and has potential as a novel MRI (magnetic resonance imaging) contrast agent [11]. In addition to its selective activation by MMP-7, PB-M7VIS includes a non-cleavable internal reference signal to provide for detection of both cleaved and uncleaved reagent. We have shown that PB-M7VIS can be used to selectively detect and assay MMP-7 *in vitro* and that it can be administered intravenously to detect tumour-associated MMP-7 activity *in vivo* using a mouse xenograft model of human colon cancer. This polymer-based fluorogenic substrate thereby serves as a PB for the detection and imaging of MMP-7 activity *in vivo*. Detection and imaging of tumour-associated MMP-7 activity, using this novel imaging reagent, makes possible not only the molecular imaging of such tumours, but also has potential for assessing the *in vivo* efficacy of MMPIs that are being tested for therapeutic treatment of several diseases.

EXPERIMENTAL

Materials

Except as noted, all chemicals and biochemicals were reagent-grade and solutions were prepared in deionized, filtered water (Milli-Q; Millipore, Billerica, MA, U.S.A.). Generation-4 Starburst® PAMAM dendrimer, Brij® 35 solution (30 %, w/v) and Tricine (> 98 %) were obtained from Sigma–Aldrich (St. Louis, MO, U.S.A.). SIA (*N*-succinimidyl iodoacetate) was obtained from Pierce Chemical (Rockford, IL, U.S.A.). Fl-M7 [Fl(AHX)RPLALWRS(AHX)C, where AHX stands for aminohexanoic acid], a fluorescein (Fl)-labelled and HPLC-purified peptide that includes two AHX linkers, was obtained from ResGen Invitrogen (Huntsville, AL, U.S.A.). TRITC [TMR (tetramethylrhodamine) β-isothiocyanate; mixed isomers], FITC, dye-quenched (DQ)-collagen and DQ-gelatin were obtained from Molecular Probes (Eugene, OR, U.S.A.). Matrigel™ was obtained from BD Biosciences (San Jose, CA, U.S.A.). MMP-2, -3 and -7 were obtained from Calbiochem (La Jolla, CA, U.S.A.). BB-94 {[4-(*N*-hydroxyamino)-2*R*-isobutyl-3*S*-(thienylthiomethyl)-succinyl]-L-phenylalanine-*N*-methylamide} was obtained from British Biotech (Oxford, U.K.). Ketamine (Ketaset) was obtained from Fort Dodge Animal Health (Fort Dodge, IA, U.S.A.) and xylaxine from Lloyd Laboratories (Shenandoah, IA, U.S.A.). SW480 human colon cancer cells were obtained from A. T. C. C. (Manassas, VA, U.S.A.). Stable clones expressing the neomycin selection cassette (SW480*neo*) or neomycin and MMP-7 (SW480*mat*) were isolated and characterized as reported previously [12]. Cells were maintained in Dulbecco's modified Eagle's medium containing 10 % (v/v) foetal calf serum at 37 °C in a 5 % CO_2 environment.

Preparation of PB-M7VIS

The fluorescent peptide–dendrimer conjugate PB, PB-M7VIS, was synthesized according to the procedure outlined in Scheme 1. The Fl-labelled peptide Fl-M7 was designed for selective cleavage by MMP-7 and to yield a relatively insoluble Fl-labelled N-terminal fragment that includes an AHX linker (Scheme 1). In the first step of the synthesis of PB-M7VIS, a methanolic solution of generation-4 Starburst® PAMAM dendrimer (14.215 kDa with 64 surface amines/polymer) was reacted with SIA. This activated PAMAM was then reacted with Fl-M7 (up to 5 equivalents/

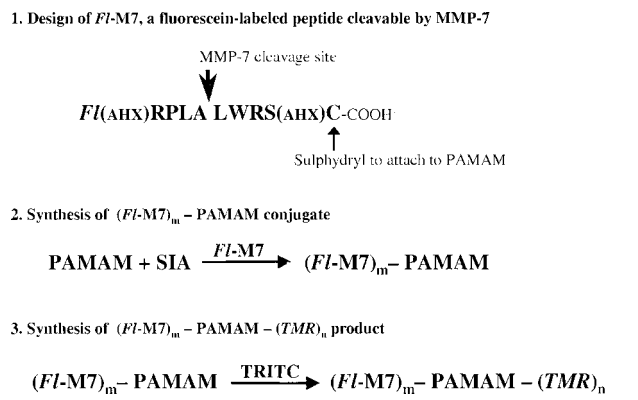

Scheme 1 Scheme for the synthesis of PB-M7VIS, a (Fl-M7)$_m$–PAMAM-(TMR)$_n$ co-polymer

Table 1 PB-M7VIS-specific PBs prepared with different ratios of Fl-M7 and TMR

PB-M7VIS was prepared with different Fl-M7/PAMAM and TMR/PAMAM ratios as indicated. The fluorescence of Fl was measured before and after cleavage by MMP-7 (see Figure 2) and is expressed as the ratio, cleaved/uncleaved.

Reagent	Fl-M7 peptide (mol/mol of PAMAM)	TMR (mol/mol of PAMAM)	Fl ratio (cleaved/uncleaved)
2-0	2.4	0	1.6
2-1	2.4	0.7	2.6
2-2	2.4	1.4	3.6
2-3	2.4	2.6	5.2
2-4	2.4	3.2	5.1
2-5	2.4	5.1	4.0
4-1	4.5	1.6	6.1
4-2	4.5	4.5	17

PAMAM) to link the peptide, through the thiol (sulphydryl) of its C-terminal cysteine residue, to the dendrimer yielding the (Fl-M7)$_m$–PAMAM conjugate, with an average of approx. 4.5 Fl-M7 linked per polymer. The (Fl-M7)$_m$–PAMAM conjugate was subsequently derivatized with different amounts of TRITC to couple TMR (up to 5 equivalents/PAMAM) with the polymer scaffold as an internal reference fluorophore. The products of these syntheses form a set of polymer-based PB-M7VIS reagents in which the Fl-M7 peptide serves as a protease-activatable optical sensor with TMR as an internal reference (Table 1). The synthesis and purification, as detailed below, were performed with minimal exposure to light.

Synthesis of (Fl-M7)$_m$–PAMAM

To synthesize the thioether-bonded conjugate (Fl-M7)$_m$–PAMAM, a methanolic solution (10 %, w/w) of PAMAM (5 mg, 0.35 μmol, equivalent to 22.5 μmol of primary amines) was diluted with methanol and aqueous EDTA to 0.3 ml [methanol/water (2:1) and 2 mM in EDTA] and activated by the addition of 11 μmol of SIA (0.1 ml of a 110 mM solution, freshly prepared in DMSO). After reaction for 2 h at ambient temperature, residual amines, as measured by the ninhydrin reaction, were approx. 50 % of those of the original dendrimer indicating an essentially quantitative reaction of SIA with PAMAM to form the product (activated PAMAM). The activated PAMAM was then immediately reacted with Fl-M7 peptide (3 mg, 1.7 μmol) that had been dissolved in methanol and diluted with aqueous EDTA (pH 8.0) to 8 mg/ml [60 % (v/v) methanol/water and 4 mM

EDTA] giving a reaction mixture with 5 mg of PAMAM and 3 mg of Fl-M7 in 775 μl (methanol/DMSO/water in the ratio 55:13:32 with 2.7 mM EDTA). After overnight incubation at ambient temperature (16–20 h in the dark), cysteine (8.8 μmol, 44 μl of 0.2 M cysteine in methanol, i.e. approximately stoichiometric with respect to SIA) was added to the reaction mixture so as to derivatize any residual iodoacetyl groups of the activated PAMAM, i.e. iodoacetyl groups that had not either reacted with the thiol of Fl-M7 or been hydrolysed. After 90 min, the reaction mixture was diluted 10-fold with a buffer (0.1M NaCl/10 mM Hepes/HCl, pH 8.0/1 mM EDTA) and then concentrated and purified by two rounds of diafiltration (CentriPrep YM-10; Millipore). The fraction of Fl-M7 peptide incorporated into the peptide-PAMAM co-polymer was calculated from the relative Fl concentration in the reaction mixture versus effluents (as measured by absorbance at 497 nm). To vary the Fl-M7/PAMAM ratio, the amount of Fl-M7 added to activated PAMAM was varied [up to a ratio of 5, yielding $(Fl\text{-}M7)_{4.5}$–PAMAM]. The product $(Fl\text{-}M7)_m$–PAMAM (80–90 % recovery of PAMAM, based on the ninhydrin assay) was stored (4 °C) at approx. 5 mg of PAMAM/ml in 50 mM Na_2CO_3 (pH 9), 1 mM EDTA overnight (or up to several weeks) and subsequently labelled with TMR as described below.

Synthesis of the $(Fl\text{-}M7)_m$–PAMAM-$(TMR)_n$ product, PB-M7VIS

To label the PAMAM scaffold of $(Fl\text{-}M7)_m$–PAMAM with different amounts of TMR, the peptide-PAMAM co-polymer [either 0.1 or 1 mg in 50 mM Na_2CO_3 and 1 mM EDTA (pH 9)] was reacted with up to six equivalents of TRITC added in DMSO. The volume of DMSO was adjusted to maintain a 1:1 DMSO/buffer ratio, with a total reaction volume of either 0.05 or 0.4 ml for 0.1 and 1.0 mg of the reaction mixture respectively. After overnight incubation at room temperature (22–24 °C), a 10-fold excess of cysteine (with respect to TRITC) was added from a 0.2 M methanolic solution. After a 2 h incubation, the reaction mixture was diluted 10-fold with 0.1 M NaCl, 5 mM Hepes and 1 mM EDTA (pH 7.0) and the product $(Fl\text{-}M7)_m$–PAMAM-$(TMR)_n$ was separated from unincorporated TMR by diafiltration (as above) by performing a total of four washes with the same buffer, except that 10 % ethanol was included in the first two washes to facilitate the removal of TMR by-products. Incorporation of TMR into the dendrimer was calculated from the relative 554 nm absorbance of the sample versus effluent. The recovery of PAMAM from diafiltration was generally 80–85 % as estimated either by ninhydrin reaction or from the Fl absorption (absorbance at 497 nm) of control $(Fl\text{-}M7)_m$–PAMAM samples not labelled with TMR. Unless noted otherwise, the concentration of $(Fl\text{-}M7)_m$–PAMAM-$(TMR)_n$ reagents was based on the PAMAM core dendrimer. These reagents were stable at 4 °C in 0.1 M NaCl, 5 mM Hepes and 1 mM EDTA (pH 7.0) (either with or without 20 % ethanol) for at least several weeks.

Control PAMAM reagents, lacking the selectively cleavable peptide but labelled on the polymer scaffold with either Fl or TMR or both (i.e. Fl-PAMAM, PAMAM-TMR or Fl-PAMAM-TMR), were prepared by reacting generation-4 PAMAM directly with either FITC or TRITC or a mixture of the two followed by diafiltration.

Ninhydrin assay for amines

To quantify the coupling reactions used for the synthesis of PB-M7VIS (see Scheme 1), the amine content of PAMAM was measured by the method of Moore and Stein [13], using the aqueous DMSO reagent [14] as follows. Samples of either standards or unknowns in a total volume of 0.2 ml of water were mixed with 0.1 ml of ninhydrin reagent solution (Sigma, St. Louis, MO, U.S.A.) in a 1.5 ml snap-top conical plastic tube that was sealed and placed in a boiling-water bath for exactly 10 min. After cooling, 0.6 ml of ethanol (95 %, v/v) was added and mixed, giving a final volume of 0.9 ml. The absorbance of the blue product was measured at 570 or 562 nm using either a dual-beam spectrometer (UV-2501PC; Shimadzu Scientific Instruments, Columbia, MD, U.S.A.) or an automated sampling photometer (BioPhotometer; Eppendorf-Netheler-Hinz, Hamburg, Germany) reading the absorbance at 562 nm. The assay was standardized with L-leucine (prepared at 0.1 M and diluted immediately before use to 1 mM in deionized water) and found to be linear at least up to 20 nmol of L-leucine, with a colour yield (absorbance at 562 nm) of approx. 0.02 $cm^{-1} \cdot nmol^{-1}$. As reported by Moore [14] for amino acids, the ninhydrin colour with PAMAM was stable after storing the reacted samples overnight at ambient temperature. On the basis of the predicted number of primary amines present in PAMAM generations 3 and 4 (32 and 64 mol of NH_2 per mol of PAMAM respectively), the ninhydrin colour yield with these two dendrimers was approx. 75 and 50 % respectively of that obtained with the L-leucine standard.

Fluorescence spectroscopy and fluorimetric assay for MMP activity

Fluorescence excitation and emission spectra of PB-M7VIS, diluted with deionized water to 0.05–0.1 μM to obtain an absorbance of < 0.05, were measured in 4 mm × 4 mm quartz cuvettes at 25 °C using an L-format QuantaMaster QM-9 photon-counting fluorimeter (1 nm steps, 2 nm slits) operated with FeliX software (Photon Technology International, Lawrenceville, NJ, U.S.A.). Fluorescence spectra of different $(Fl\text{-}M7)_m$–PAMAM-$(TMR)_n$ reagents recorded before and after treatment with MMP-7 are illustrated with the same amplitude after cleavage to account for differences in the Fl concentration of each sample. To measure the rate of proteolysis of PB-M7VIS, an aliquot (3 μl) of either active MMP-7 (2 ng/μl), MMP-2 (7 ng/μl) or MMP-3 (5 ng/μl) was added to the reagent diluted to 0.2 μM in Tricine buffer (50 mM Tricine, pH 7.4/0.2 M NaCl/10 mM $CaCl_2$/50 μM $ZnSO_4$/0.005 % Brij 35), at 72 μl/well in a white 96-well Microfluor-1 plate. Fluorescence of both Fl (λ_{ex}, 485 nm and λ_{em}, 538 nm, where λ_{ex} and λ_{em} stand for excitation and emission respectively) and TMR (λ_{ex}, 530 nm; λ_{em}, 584 nm) were measured, at 37 °C, as a function of time (MFX microtitre plate fluorimeter; Dynex Technologies, Chantilly, VA, U.S.A.). Samples were measured in triplicate and the enzymic activity was calculated from the initial rate of increase in Fl fluorescence (measured in arbitrary units), defining the increase in Fl fluorescence at the plateau value (usually attained within 3 h) to be equivalent to complete cleavage of the substrate. Inhibition was tested by inclusion of either 30 mM EDTA or 10 μM BB-94, a broad-spectrum MMPI [15], in the assay. With MMP-7, the k_{cat}/K_m value for PB-M7VIS was calculated by non-linear regression (GraphPad Prism; GraphPad Software, San Diego, CA, U.S.A.) of the activity data by varying the PB-M7VIS concentration from 0.1 to 1.0 μM; double-reciprocal $1/v$ versus 1/[S] Lineweaver–Burk plots [16] gave a similar k_{cat}/K_m value. With MMP-2 and -3, the activity was low and the k_{cat}/K_m values were calculated from the average of at least three activity measurements at 0.2 μM substrate, assuming $[S_o] \ll K_m$, such that $k_{cat}/K_m = v/[S_o][E_o]$, as described in [17]. All the three MMPs (-2, -3 and -7) were each confirmed to be active in Tricine buffer with either DQ-gelatin or DQ-collagen IV (Molecular Probes), known substrates for these MMPs. Cleavage of PB-M7VIS was also tested with bacterial collagenase (type IV), trypsin, proteinase K and non-specific protease from *Streptomyces griseus* (pronase E,

type XIV), each obtained from Sigma–Aldrich; for these proteinases, activity was calculated per μg and is expressed relative to the activity of MMP-7.

Optical imaging system and calibration

Quantitative fluorescence imaging was achieved by taking digital pictures with a full-frame, black and white CCD (charge-coupled-device) camera (MicroMax 1317-K/1; Princeton Instruments, Trenton, NJ, U.S.A.) coupled with a fluorescence microscope with a variety of Plan-Neofluar objective lenses (Axiophot; Carl Zeiss, Thornwood, NY, U.S.A.) as specified. Camera control, image acquisition and analyses were performed using MetaMorph imaging software (Universal Imaging, Downington, PA, U.S.A.). Fluorescence signal was linear with camera exposure time and exposure conditions were optimized for maximum dynamic range. Generally, images were focused and the specimen field was orientated under low-intensity white light before fluorescence excitation. Two to three images were then acquired to bracket optimal exposure times up to 30 s. Light was collected through one of two low magnification objectives, depending on whether the measurement was for a calibration sample or for the intact mouse as described below. In either case, the Fl signal (green channel, 500–530 nm emission) was discriminated using a green band-pass filter set (41025; Chroma Technology Corp., Brattleboro, VT, U.S.A.) and the rhodamine signal (red channel, >570 nm emission) was discriminated using a red long-pass filter set (41032; Chroma Technology Corp.). The green channel selectively detects Fl fluorescence from PB-M7VIS with only background signal from PAMAM-TMR, although only a part of the total Fl emission band can be acquired. Thus the microscope imaging system gives different Fl/TMR ratios compared with those calculated from corrected spectral amplitudes measured in a fluorimeter, since the long-pass filter in the red channel detects a larger fraction of the total TMR fluorescence compared with the relatively narrow Fl fluorescence band collected through the green channel. This condition limits the dynamic range compared with the fluorimeter experiment, but it allows effective signal discrimination in the presence of both dyes. The difference in sensitivity of the two channels is, in part, compensated for by increasing the green-channel exposure with respect to the red channel, e.g. 10 and 1 s respectively. This two-colour microscope imaging system was calibrated with a set of PB-M7VIS samples consisting of mixtures of uncleaved and MMP-7-cleaved reagent, 0.2 nM in Tricine buffer + 20 mM EDTA, loaded into capillaries (0.75 mm borosilicate glass; World Precision Instruments, Sarasota, FL, U.S.A.). Each capillary sample of PB-M7VIS, as well as duplicate control capillaries, was imaged in at least triplicate (10 and 1 s for green and red channels respectively) using a $10\times$/0.50 Plan-Neofluar objective to measure the fluorescence intensity in each channel as a function of the extent of cleavage of PB-M7VIS. The intensity was calculated as the average counts/pixel after subtraction of background signals from control capillaries containing only Tricine buffer plus 20 mM EDTA and expressed as the means $\pm$ S.E.M. from three or more images of each sample.

For subcutaneous detection and imaging of PB-M7VIS, samples of either uncleaved or MMP-7-treated reagent in Tricine buffer + 30 mM EDTA were each diluted 10-fold into Matrigel™ at 4 °C, and 100 μl aliquots were injected subcutaneously into several sites along the back of a freshly killed nude mouse. The injected samples were visible as fluorescent phantoms below the skin and each was imaged in at least triplicate in both green and red channels of the microscope imaging system using a $2.5\times$/0.075 Plan-Neofluar objective (field, approx. 10 mm^2). In these studies, pretreatment of the mouse skin with glycerol significantly improved contrast by decreasing the background from scattering (see [18]) of excitation light from the mouse skin by approx. 30 % (both in the red and green channels). The glycerol treatment also increased the dynamic range for the fluorescent phantoms by approx. 20–30 %, indicative of a decrease in excitation and emission scattering. Photobleaching was negligible in these experiments.

In vivo detection and imaging of MMP-7 activity

Control and MMP-7-expressing xenograft tumours were established on the flanks of athymic nude mice (Harlan, Indianapolis, IN, U.S.A.) by subcutaneous injection of 1×10^6 cells, either SW480*neo* or SW480*mat*. After tumours of approx. 1–2 cm had developed (4–6 weeks), the animals were anaesthetized (ketamine/xylaxine, 145 and 14.5 mg/kg respectively, prepared in sterile saline and administered intraperitoneally) and images were recorded over both tumours as well as over a non-tumour area between the xenografts, by integration for up to 10 s in the green and red channels of the microscope imaging system described above. Before imaging, the area of the skin to be imaged was treated with glycerol. PB-M7VIS (1.6 nmol in 150 μl of sterile 0.9 % saline) was then injected into the retro-orbital venous bed of one eye and the animal re-imaged for up to approx. 30 min post-injection. Additional image sets of the re-anaesthetized animal were recorded at approx. 2 and 24 h post-injection of the PB-M7VIS, the animal was then killed. *In vivo* results were from six animals, each bearing control and MMP-7-expressing xenograft tumours. Three of these animals were treated with BB-94, administered in PBS containing 0.01 % Tween 20, at 35 mg/kg by intraperitoneal injection once every 24 h (a total of three doses over 48 h) and imaged both before and within 2 h after the final treatment with BB-94. All animal experiments were in accord with IACUC regulations. The tumour and non-tumour image data sets were analysed using MetaMorph to measure fluorescence in the green and red channels after subtraction of instrument background signals. To validate the green- and red-channel background corrections, each set of data included one or more images at the edge of the imaging field to collect data simultaneously from both the tumour and the black background material. Multiple images of adjacent regions of mouse skin (either over individual tumours or over non-tumour areas) exhibited <7 % and approx. 14 % image-to-image variation in average fluorescence in the green and red channels respectively. For statistical analyses using either paired *t* test, WSR (Wilcoxon Sign Rank) or Sign tests, the fluorescence from the SW480*neo* and SW480*mat* tumours was compared after subtraction of the non-tumour background fluorescence in the green and red channels respectively.

RESULTS

Preparation and fluorescence properties of PB-M7VIS

The polymer-based PB, PB-M7VIS, was constructed on a dendrimeric scaffold (Starburst®; generation-4) with both an optical protease sensor (Fl-M7) and an internal reference, TMR, according to the procedure outlined in Scheme 1. The peptide sequence of Fl-M7 is based on a fluorogenic peptide that was optimized for MMP-7 [10]. For the first step of the synthesis to form the $(\text{Fl-M7})_m$–PAMAM conjugate, approximately half of the terminal amines of PAMAM were activated by reaction with SIA, a step that was essentially quantitative, as determined by ninhydrin assay of the fraction of amines remaining in activated

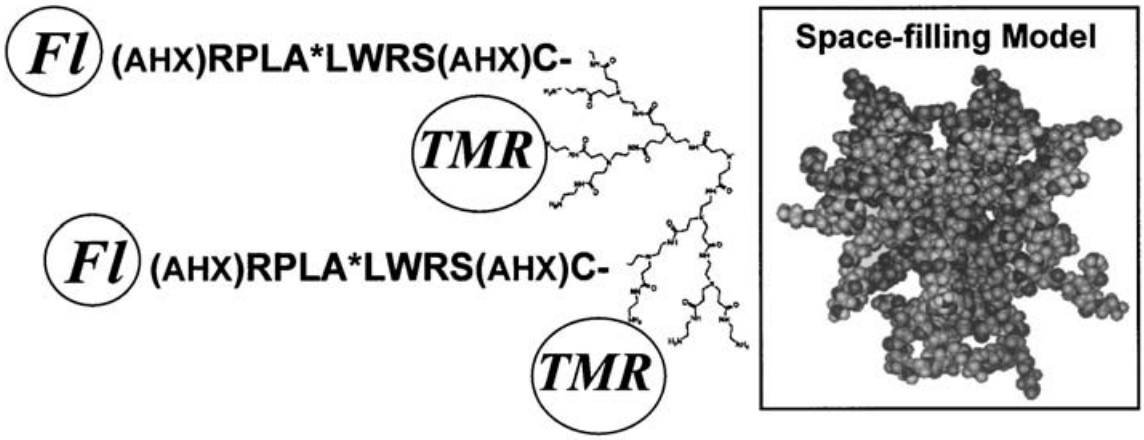

Figure 1 Schematic structure of the polymer-based PB, PB-M7VIS, designed as a fluorogenic substrate for MMP-7

The Fl optical sensor is linked via AHX to the N-terminus of the MMP-selective cleavable peptide (RPLA*LWRS, with MMP-7-cleavage site denoted by an asterisk) that is coupled via a second AHX and C with the dendrimeric polymer. The internal reference, TMR, of PB-M7VIS is linked directly to the dendrimer (Starburst® PAMAM dendrimer, generation-4), depicted both by partial structure and in the space-filling model (modified from Dendritech Inc.™ available at www.dendritech.com).

PAMAM (results not shown). The subsequent incorporation of Fl-M7 to form the $(Fl\text{-}M7)_m$–PAMAM conjugate also proceeded efficiently ($83 \pm 10\%$, means $\pm$ S.E.M., $n = 4$). The efficiency of TMR incorporation into $(Fl\text{-}M7)_m$–PAMAM varied over the range 40–80%, which appeared to depend on the freshness of the TRITC reagent. The product of this reaction is $(Fl\text{-}M7)_m$–PAMAM-$(TMR)_n$. By varying the ratio of the Fl-M7 and TMR components with respect to the PAMAM scaffold, a set of such reagents was obtained (Table 1) that are collectively referred to as PB-M7VIS, the structure of which is illustrated in Figure 1.

PB-M7VIS reagent was prepared at two Fl-M7/polymer ratios and each of these preparations was derivatized with different amounts of TMR (Table 1). After preparation, the different PB-M7VIS reagents exhibit different Fl fluorescence signals (Figure 2, spectra a, c and e). However, after treatment with MMP-7, the Fl spectral amplitude of these PB-M7VIS preparations is similar when normalized with respect to the Fl-M7 concentration (Figure 2, spectra b, d and f) and is comparable with that of the same concentration of Fl-M7 alone (results not shown). The relative increase in amplitude of the Fl signal after treatment with MMP-7 is dependent on both the Fl-M7/PAMAM and TMR/PAMAM ratios (Figure 2 and Table 1). In the absence of TMR (reagent 2-0, Table 1), treatment with MMP-7 yields an approx. 1.6-fold increase in Fl-fluorescence (Figure 2, spectra a and b). The addition of 1.4 equivalents of TMR (reagent 2.2) results in a significant increase in the Fl fluorescence enhancement after MMP-7 treatment (ratio of 3.6; Figure 2, spectrum c versus spectrum d; and Table 1). Increasing the Fl-M7/PAMAM ratio (reagent 4-1 versus 2-2) results in a further enhancement of the Fl fluorescence ratio (approx. 6 in reagent 4-1; Figure 2, spectra e and f), which can be attributed to additional Fl to Fl homotransfer and self-quenching in this reagent (with an average of 4.5 Fl-M7/polymer). At this Fl-M7/PAMAM ratio, increasing the amount of TMR (reagent 4-2 versus 4-1, Table 1) gives a further enhancement of the cleaved/uncleaved ratio of Fl fluorescence (to 17; Table 1) referable to additional Fl to TMR resonance energy transfer quenching of the Fl fluorescence in this reagent. After preparation, PB-M7VIS reagent 4-2 exhibits approx. 6% of the Fl fluorescence of Fl-M7 alone and, after treatment with MMP-7, exhibits similar amplitudes of its Fl and TMR spectral components (results not shown). In subsequent

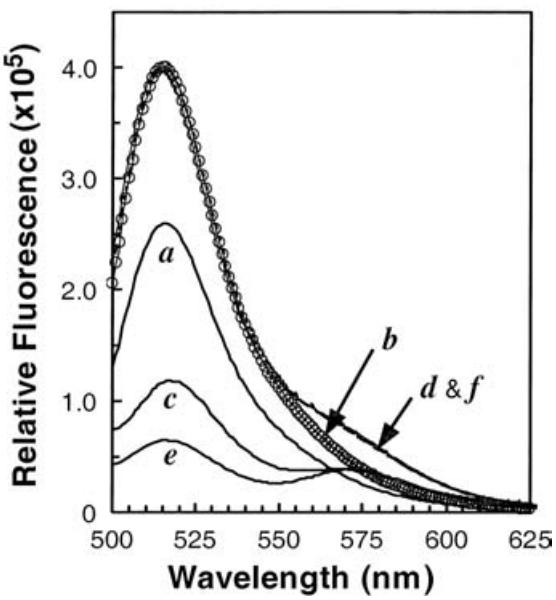

Figure 2 Effect of Fl and TMR labelling ratios on the Fl fluorescence of selected PB-M7VIS reagents

Fluorescence emission spectra (λ_{ex}, 493 nm), both before (spectra a, c and e) and after (spectra b, d and f) treatment with MMP-7, of PB-M7VIS reagents 2-0 (0.1 μM, spectra a and b, the latter depicted with ○), 2-2 (0.1 μM, spectra c and d) and 4-1 (0.05 μM, spectra e and f). The amplitudes of spectra b, d and f were similar and, for comparison, the spectra paired before and after for each reagent were scaled to the same amplitude after treatment.

in vitro and *in vivo* studies, PB-M7VIS refers to reagents 4-1 and 4-2 respectively.

The fluorescence spectra of PB-M7VIS resolve both optical components (Fl, $\lambda_{em,max}$, 517 nm and TMR, $\lambda_{em,max}$, 572 nm; Figure 3A). The Fl emission spectrum (Figure 3A, spectrum 2) exhibits a significant shoulder at 572 nm, indicative of resonance energy transfer from Fl to TMR in PB-M7VIS. After treatment with MMP-7, the amplitudes of the Fl excitation and emission spectra (Figure 3B, spectra 5 and 6 respectively) increase significantly, whereas there is a minimal change in the amplitude of

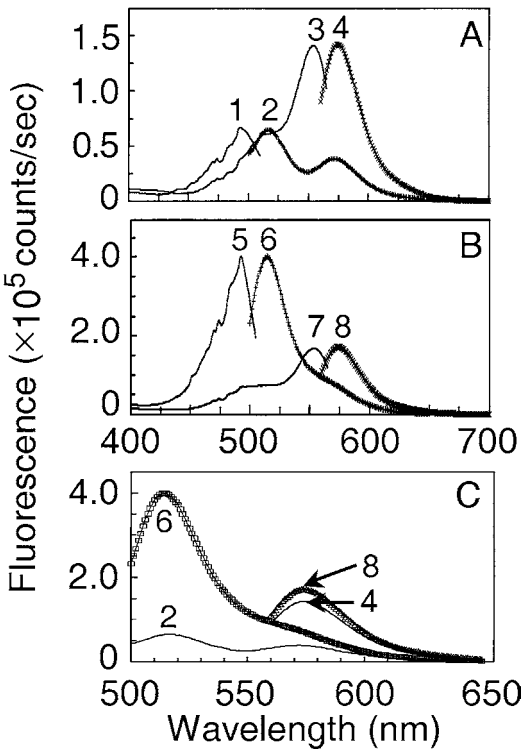

Figure 3 Fluorescence spectra for an optimized PB-M7VIS reagent both before and after treatment with MMP-7

(**A**, **B**) Fluorescence excitation spectra (λ_{em}, 517 nm, spectra 1 and 5 or λ_{em}, 572 nm, spectra 3 and 7) and emission spectra (λ_{ex}, 493 nm, spectra 2 and 6 or λ_{ex}, 554 nm, spectra 4 and 8) of PB-M7VIS (reagent 4-1, Table 1) before treatment (**A**) and after treatment (**B**) with MMP-7 (note the change in scale). (**C**) Fl fluorescence emission spectra (λ_{ex}, 493 nm) of PB-M7VIS reagent 4-1 (spectra 2 and 6) compared with the TMR emission (λ_{ex}, 554 nm; spectra 4 and 8) before treatment (spectra 2 and 4) and after treatment (spectra 6 and 8, □ and △ respectively) with MMP-7.

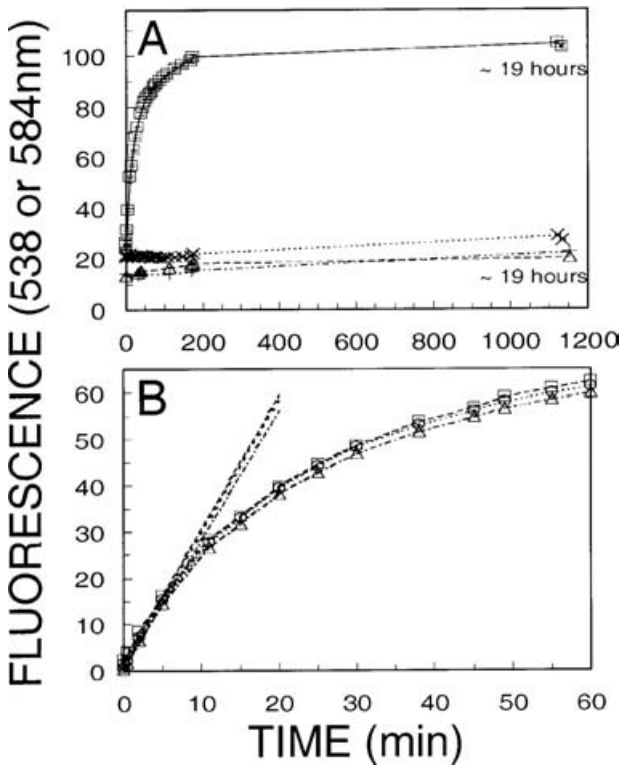

Figure 4 PB-M7VIS, a fluorogenic substrate for MMP-7

PB-M7VIS was incubated (37 °C) with MMP-7 in the absence (□ and △) or presence (× and +) of EDTA, measuring the fluorescence (microtitre plate fluorimeter) of both Fl (λ_{ex}, 485 nm; λ_{em}, 538 nm) (□ and ×) and TMR (λ_{ex}, 530 nm; λ_{em}, 584 nm) (△ and +) at the times indicated (see the Experimental section). (**A**) Fl and TMR fluorescence (± EDTA; means ± S.E.M., $n = 3$). For clarity, the TMR data are plotted after subtraction of 5 fluorescence units. (**B**) Three individual Fl data sets (first hour, control subtracted, for the data averaged in **A**). The initial specific activity of MMP-7 in these assays, calculated from the initial slope of the increase in Fl fluorescence, is 78 ± 1 pmol · min^{-1} · μg^{-1} (mean ± S.E.M.).

the TMR spectra (Figure 3B, spectra 7 and 8). Comparison of the amplitudes of the emission spectra of PB-M7VIS before and after treatment with MMP-7 (Figure 3C) shows that the Fl fluorescence signal (Figure 3C, spectra 2 and 6) functions as an optical sensor to detect proteolysis of the Fl-M7 peptide, whereas the TMR fluorescence (Figure 3C, spectra 4 and 8) serves as an internal reference to monitor the total (cleaved and uncleaved) concentration of the reagent, consistent with the original design of this PB.

In vitro assay of MMP activity with PB-M7VIS and specificity for cleavage

The increase in Fl fluorescence observed in the fluorescence spectra of PB-M7VIS was measured as a function of time after the addition of MMP-7 to detect and measure the rate of cleavage of the Fl-M7 peptide substrate component of the polymeric reagent (Figures 4A and 4B). After the addition of MMP-7, there is a rapid increase in the Fl fluorescence to a plateau value that is stable for up to at least 19 h (Figure 4A). The approx. 5-fold increase in Fl fluorescence is comparable with that observed in the fluorescence spectra of this reagent (Table 1) and is inhibited either by EDTA (Figure 4A) or by BB-94, the broad-spectrum MMPI (results not shown), consistent with metalloproteinase activity. In contrast, the TMR fluorescence of PB-M7VIS does not change appreciably after the addition of MMP-7 either in the presence or absence of EDTA (Figure 4A). In addition, control experiments with Fl-PAMAM-TMR reagents lacking the peptide component of Fl-M7 showed no change in either Fl or TMR fluorescence after the addition of MMP-7 (results not shown). The increase in Fl fluorescence of PB-M7VIS after the addition of MMP-7 is therefore attributed to proteolytic cleavage of the Fl-M7 component of the reagent. The initial rate of increase in either the Fl fluorescence or the Fl/TMR ratio (results not shown) is used to calculate enzymic activity with minimal well-to-well variability (Figure 4B). With MMP-7, the k_{cat}/K_m value for PB-M7VIS (Table 2) was calculated from sets of MMP-7 activity measurements as a function of substrate concentration (results not shown) and is comparable with that for the soluble peptide (dinitrophenyl-RPLAWRS) (1.9×10^5 M^{-1} · s^{-1} at 30 °C)

Table 2 Selective cleavage of PB-M7VIS by MMP-7

The k_{cat}/K_m values (means ± S.E.M.) with PB-M7VIS substrate were determined (see the Experimental section) from two or more independent triplicate sets of fluorescence activity assays (see Figure 4) with MMPs that were shown to be active with DQ-gelatin and/or DQ-collagen substrates.

Enzyme	k_{cat}/K_m (M^{-1} · s^{-1})
MMP-7*	$1.9 \pm 0.2 \times 10^5$
MMP-2	$3.4 \pm 1.5 \times 10^3$
MMP-3	$1.5 \pm 0.5 \times 10^4$

* With MMP-7, the K_m value for PB-M7VIS is 0.5 ± 0.1 μM.

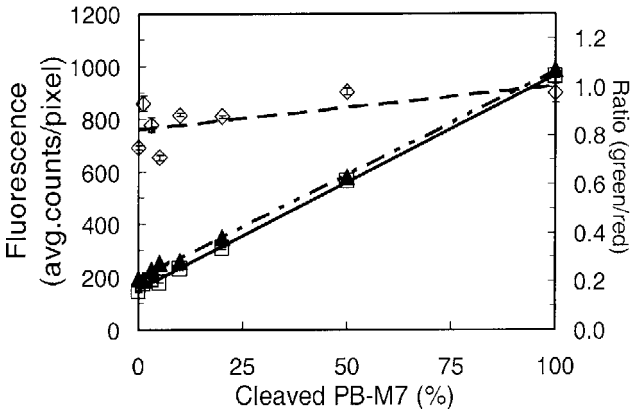

Figure 5 Imaging calibration of microscope CCD camera to measure the proteolytic cleavage of PB-M7VIS

A set of PB-M7VIS samples containing the indicated percentage of (MMP-7)-cleaved and -uncleaved reagents were prepared in capillaries and analysed in the *in vivo* optical imaging system described in the Experimental section, measuring both the green (*Fl*, ▲) and red (TMR, ◇) fluorescence (10 and 1 s respectively) as a function of the proteolytic cleavage of PB-M7VIS. The ratio of Fl to TMR is plotted (□). Linear regression of the Fl and Fl/TMR ratios each yield $r^2 > 0.99$.

[10]. The measured K_m value of MMP-7 for PB-M7VIS was 0.5 μM. The efficient cleavage of PB-M7VIS by MMP-7 as reflected by its relatively high k_{cat}/K_m value is similar to those of the best MMP-7 peptide substrates identified by phage display methodology [19].

The specificity of PB-M7VIS was tested by comparing the efficiency of cleavage of PB-M7VIS by MMP-7 with the proteolysis by MMP-2 (gelatinase A) or MMP-3 (stromelysin 1) or by some general proteinases. PB-M7VIS was readily cleaved by the non-specific protease (pronase E) at approx. 40 % of the rate of cleavage by MMP-7, but more slowly by trypsin or proteinase K (approx. 5–10 % of the rate of cleavage by MMP-7) and only poorly by bacterial collagenase (approx. 1 % of the MMP-7 rate; results not shown). With MMP-2 or -3, there was a relatively slow increase in the Fl fluorescence of PB-M7VIS, indicative of cleavage of the substrate (results not shown). The k_{cat}/K_m value for PB-M7VIS was approx. 56- or 13-fold lower for MMP-2 and -3 respectively when compared with MMP-7 (Table 2). Control experiments showed that these enzyme preparations were active against gelatin or collagen substrates. Whereas MMP-2, -3 and -7 have been reported to exhibit some overlap in substrate specificity [1,20], PB-M7VIS exhibits selective cleavage by MMP-7. The approx. 13-fold more efficient cleavage of PB-M7VIS by MMP-7 when compared with MMP-3 is approx. 3-fold more selective than was found in peptide substrates identified by phage display [19]. Although Fl-M7 includes the $PXXX_{Hy}$ motif that can be efficiently cleaved by MMP-2 [21], this peptide on the polymer host in PB-M7VIS appears to be a poor substrate for MMP-2, with approx. 60-fold less efficient cleavage than by MMP-7. The presence of the relatively large hydrophobic residue, L, at the P^2 site in Fl-M7 may diminish interaction with MMP-2, which has been shown to favour smaller residues at this position [21].

In vivo imaging of tumour-associated MMP-7 activity via fluorescence of cleaved PB-M7VIS

The green (Fl) and red (TMR) channels of the *in vivo* optical imaging system were calibrated by measuring the fluorescence of a set of PB-M7VIS samples prepared with different ratios of cleaved to uncleaved reagent (Figure 5). The exposure time of the imaging system camera was adjusted to yield similar signal levels (equivalent dynamic range) in the green (10 s) and red (1 s) channels for the fully cleaved PB-M7VIS reagent. The green fluorescence increases linearly with the percentage of cleaved PB-M7VIS, with little change in the red fluorescence (approx. 5-fold increase in green fluorescence compared with approx. 10 % increase in the red fluorescence). These results indicate that fluorescence in the red channel of the imaging system can be used to monitor the total concentration of PB-M7VIS, whereas either the green fluorescence directly or the green/red fluorescence ratio can be used to detect and measure the cleaved reagent in the same imaged area.

The uncleaved and cleaved PB-M7VIS can be detected and distinguished by fluorescence imaging after subcutaneous injection into a nude mouse (Figure 6). Figure 6 (upper panel, A1–B3) depicts fluorescence images in both the red and green channels for either uncleaved (panels A2 and B2) or MMP-7-treated (panels A3 and B3) PB-M7VIS compared with a control injection (Matrigel™ devoid of reagent, panels A1 and B1). Plots of typical line segments through each of these images are shown in panels C1–C3. Images of both the uncleaved and cleaved PB-M7VIS show a similar fluorescence in the red channel (approx. 400 counts/pixel, panels C2 and C3), which is approx. 4-fold the background red-channel fluorescence (approx. 100 counts/pixel, panel C1). In contrast, the green-channel fluorescence amplitude for the uncleaved reagent (panels B2 and C2) is comparable with that observed in the control (panels B1 and C1), whereas the green fluorescence of the cleaved reagent is readily detected (panel B3) with an amplitude comparable with the red fluorescence (panel C3). From the integrated background-corrected intensities of the imaged subcutaneous reagent, the green/red channel fluorescence ratios are 0.11 and 1.04 for uncleaved and cleaved PB-M7VIS respectively, and in the same range as those observed in the calibration (Figure 5). These results indicate that the skin of a nude mouse does not markedly affect the relative detection of the green and red fluorescence signals from PB-M7VIS.

To detect tumour-derived MMP-7 activity *in vivo*, a bolus (1.6 nmol) of PB-M7VIS was injected into the retro-orbital venous bed of a nude mouse carrying two kinds of xenograft tumour, either SW480*mat* (expressing MMP-7) or SW480*neo* (control), each originally derived from SW480 human colon cancer cells. The skin of the mouse over each tumour and a non-tumour dorsal area between the tumours (Figures 7A–7D) were imaged in both green and red channels both before injection and, with time, after injection. Typical results are provided in Figure 7 and Table 3. The green-channel fluorescence (Figure 7E) from images of the control tumour (Figure 7B) are essentially the same as the fluorescence from non-tumour images (Figure 7C). In contrast, the green-channel images of the SW480*mat* tumour (Figure 7D) that expresses MMP-7 exhibit significantly higher fluorescence when compared with images of either of the controls (Figures 7B and 7C). Fluorescence images recorded before versus 15 min after injection of PB-M7VIS show no significant difference in green-channel fluorescence, which increases only over the MMP-7-expressing tumour in the images recorded 2 h after injection of the PB (Table 3). At 24 h post-injection, images from the two tumours and from control non-tumour areas showed, within error, the same green fluorescence, although this had increased by approx. 45 % compared with the initial control value (see footnotes to Table 3). This increase in green fluorescence at 24 h probably reflects a general increase in the background fluorescence from the mouse, rather than being referable to cleaved PB-M7VIS. In this regard, there was considerable mouse-to-mouse variation in the level of background green fluorescence (see footnotes to

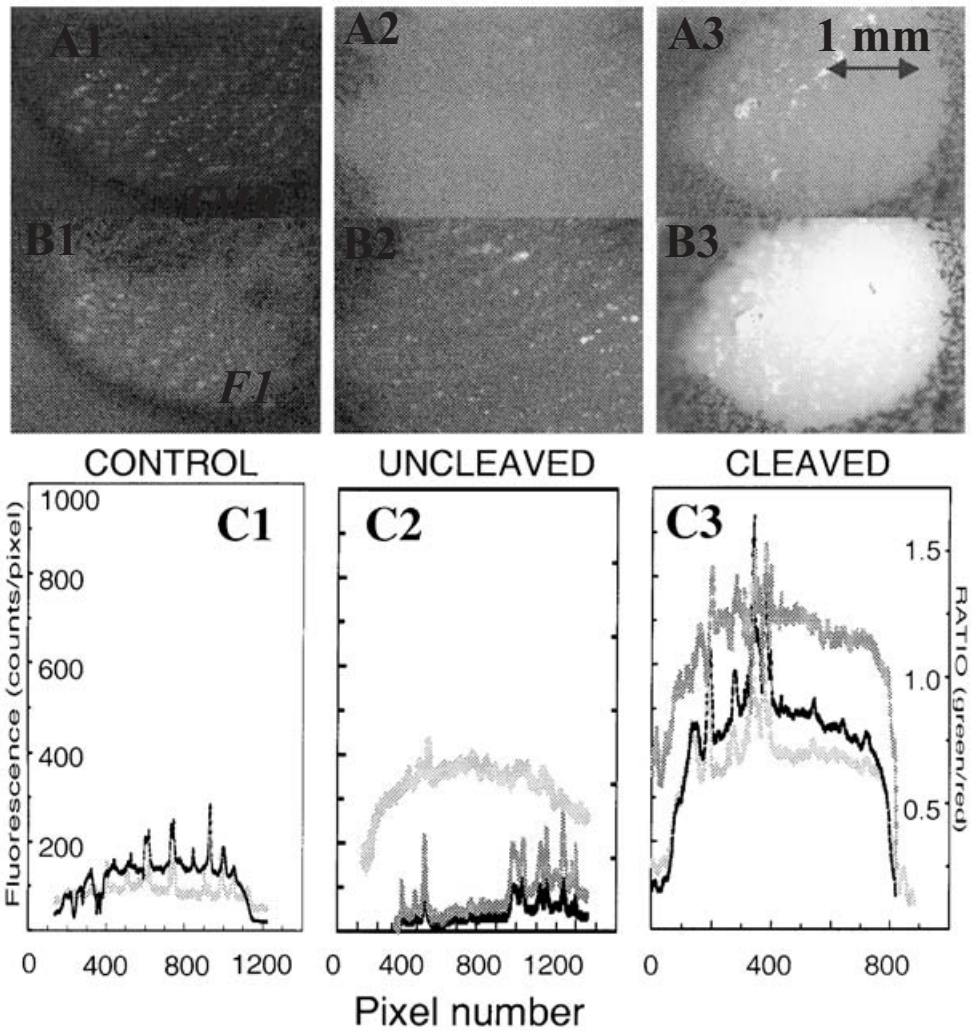

Figure 6 Quantitative fluorescence imaging of subcutaneous PB-M7VIS, either uncleaved or cleaved in a mouse

Aliquots (approx. 100 μl each in Matrigel™) of either uncleaved PB-M7VIS (images **A2** and **B2**) or cleaved PB-M7VIS (images **A3** and **B3**) or Matrigel™ alone as a negative control (images **A1** and **B1**) were injected subcutaneously in an euthanized mouse and imaged by fluorescence in either the green or red channel (**A1**–**A3** and **B1**–**B3** respectively). (**C2**, **C3**) Representative line-segment traces of the red (total substrate, **A**; light grey line) and green (cleaved substrate, **B**; black line) channels and the green/red ratio (medium grey line) are shown. The average ratio values, calculated from the integrated background-corrected intensities, are 0.11 and 1.04 for uncleaved and cleaved PB-M7VIS respectively.

Table 3) that may, in part, derive from differences in the efficacy of glycerol treatment to suppress the backscatter [18] and/or to variable autofluorescence, both of which appear to contribute to this background signal. Despite this mouse-to-mouse variation in background fluorescence, each of the six mice exhibited, at 2 h post-injection of PB-M7VIS, a significantly enhanced green fluorescence in images over the SW480*mat* tumours [668 ± 92 counts $\cdot$ $(10\ s)^{-1}$ $\cdot$ pixel^{-1}]. In contrast, the average of the green-channel fluorescence from over the control SW480*neo* tumours (three animals) was only slightly above and not significantly different from that from the control (non-tumour) region (Table 3). Statistical analysis of results from the six animals (paired t test or WSR test) shows a significant difference ($P < 0.0001$ or $P < 0.028$ respectively) between the green-channel fluorescence from the SW480*mat* tumour versus the control (SW480*neo*) tumour. Red-channel images generally exhibited similar image-to-image fluorescence intensity and relatively small changes over time (Table 3). In two of the three experiments, shortly after administration of the reagent, there appears to be an increase in red-channel fluorescence, particularly in images over each of the tumours. This increase in red fluorescence may be referable to fluorescence of TMR from the injected PB-M7VIS being distributed through the circulation. After 2 h, the enhanced red-channel fluorescence persists in control tumour images (Table 3), consistent with this tumour being accessible to the PB-M7VIS reagent and perhaps being retained therein. At the 2 h time point, the TMR fluorescence decreases in the MMP-7-positive tumour, presumably owing to wash out of the cleaved PAMAM-TMR dendrimer core. However, the red-channel fluorescence signals are relatively weak as compared with the green fluorescence and were not reproduced in all three animals, leaving open the possibility that the concentration of PAMAM-TMR (either as the uncleaved substrate, PB-M7VIS or cleaved product) is insufficient for reliable detection of this component in this experimental system. Studies of animals with comparable SW480*neo* and SW480*mat* subcutaneous xenograft tumours showed a similar accessibility of both tumours to an MRI imaging agent introduced into the vasculature via the retro-orbital

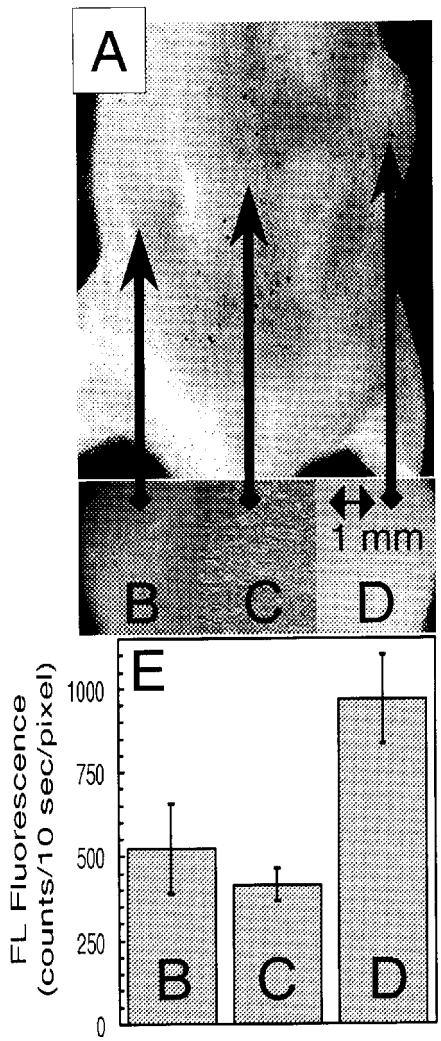

Figure 7 Detection of MMP-7 activity *in vivo* by quantitative fluorescence imaging of mouse subcutaneous xenograft tumours using PB-M7VIS

Subcutaneous injection into nude mice of either SW480*neo* or SW480*mat* cells resulted in xenograft tumours within 4–6 weeks, VISible externally in the dorsal, caudal view of the mouse (**A**, inverse image). The areas (approx. 10 mm^2 each) corresponding to both these tumours (SW480*neo* and SW480*mat*, in images **B** and **D** respectively) and a non-tumour region (image **C**) were each imaged in both green and red channels (1.36×10^6 pixels/image) at various times after retro-orbital intravenous injection of PB-M7VIS (1.6 nmol). (**E**) The bar graph depicts the average intensity $\pm$ the intensity S.D. in the green channel [counts $\cdot$ (10 s)$^{-1}$ $\cdot$ pixel^{-1}] for a typical set of CCD images [left to right: SW480*neo*, control (non-tumour) and SW480*mat*] obtained at 2 h post-injection of PB-M7VIS.

vascular bed, i.e. MRI with Magnevist (Gd^{3+}-chelate) contrast agent showed equivalent contrast in both xenograft tumours (J.O. McIntyre and M. Lepage, unpublished work). Therefore the detection of enhanced Fl fluorescence over the SW480*mat* tumour after intravenous administration of PB-M7VIS can be attributed to the MMP-7 that is expressed by this tumour rather than to the differential accessibility of this optical molecular imaging contrast reagent to the two tumours.

Treatment of the tumour-bearing mice with the MMPI BB-94 for 2 days resulted in a marked decrease in Fl fluorescence over the SW480*mat* tumour to approx. 40% of that before treatment, without any effect on the Fl fluorescence detected over the control SW480*neo* tumour (Figure 8). Thus the minimal fluorescence detected over the control tumours is not significantly different from the background (Figures 7 and 8), is not affected by treatment with the broad-spectrum MMPI (Figure 8) and, therefore, is not referable to MMP activity. After BB-94 treatment, the residual fluorescence over the SW480*mat* tumour remains somewhat higher than, but not significantly different ($P > 0.35$) from, the fluorescence over the SW480*neo* control tumour. These results are consistent with the idea that at least a major portion of the SW480*mat* tumour-associated Fl fluorescence is due to MMP activity that can be inhibited by BB-94 treatment.

DISCUSSION

The PB-M7VIS reagent described in the present study is the first MMP-7-selective proteolytic substrate designed for the *in vivo* detection and imaging of MMP-7 activity. Further, it is, to our knowledge, the first reported peptide-dendrimer co-polymer, although fluorescence-labelled PAMAM dendrimers have been described previously [22]. In PB-M7VIS, the Fl-M7 peptide serves as an MMP-7-selective optical sensor of proteolytic activity that exhibits a severalfold enhancement in Fl fluorescence after protease treatment, whereas the longer-wavelength TMR serves as an internal reference to monitor both the uncleaved and cleaved reagents. PB-M7VIS thereby functions as a PB to detect and image MMP-7 activity. Although the k_{cat}/K_m value for enzymic cleavage of PB-M7VIS by MMP-7 is comparable with that reported for the soluble fluorescent peptide [10], the recombinant enzyme in the previous study had a k_{cat} value (measured at up to 0.3 mM peptide substrate) approx. two orders of magnitude higher than that of the enzyme in the studies reported here, as measured with the polymer-based substrate PB-M7VIS. This difference in k_{cat} values may reflect a difference in the catalytic activities of the enzyme preparations used in the two studies and/or an intrinsically lower maximal turnover rate with the polymer versus peptide substrate. In contrast, in the present study, the K_m value of approx. 0.5 μM for PB-M7VIS approaches two orders of magnitude lower than that reported for the soluble peptide (26 μM) [10], indicating a higher-affinity interaction of the enzyme with the polymer-linked peptide when compared with the soluble peptide. Part of this difference can be accounted for by the presence of an average of 4.5 peptide substrates/PB-M7VIS polymer molecule. However, when this is taken into account (giving a calculated K_m value of 1.8 μM with respect to the peptide on PB-M7VIS), the difference in K_m value for the polymer versus peptide forms of the substrate remains significant, i.e. $>$10-fold. Although the differences in kinetic parameters in the two studies may in part derive from differences in the enzyme preparations and/or assay conditions, the 10-fold higher affinity of MMP-7 for PB-M7VIS compared with that reported for the peptide substrate indicates a more efficient interaction of the enzyme with the polymer. This preferred interaction of MMP-7 with the polymer-linked peptide in PB-M7VIS may reflect the nature of its natural substrates, e.g. polymeric components of the matrix and cell-surface signalling molecules that also serve as substrates [1,2,23]. Although PB-M7VIS can be cleaved by some general proteinases, it is a much poorer substrate for MMP-2 and -3, that cleave the reagent less efficiently than does MMP-7 (approx. 56- and 13-fold lower k_{cat}/K_m values respectively when compared with MMP-7). Results from the imaging studies indicate that the efficient cleavage by MMP-7 is at least sufficient for selectively detecting tumour-associated MMP-7 activity *in vivo*.

For *in vivo* imaging, a single bolus of PB-M7VIS was used at an amount giving an initial circulating concentration over the range of approx. 1 μM, based on an estimated circulating blood volume of 1.8 ml (calculated assuming 72 ml/kg [24]). The use of this relatively low dose of the beacon, at an initial concentration

Table 3 Time-dependent fluorescence imaging detection of PB-M7VIS cleavage *in vivo*

Fluorescence intensities (counts/pixel) were measured in the green (10 s) and red (3 s) channels of images of either non-tumour (the back between tumours) or *neo*-tumour or *mat*-tumour regions of an anesthetized live mouse carrying bilateral xenograft tumours (SW480*neo* and SW480*mat*) (see Figure 7). Results are expressed as the average intensity ± the intensity S.D. (after correction for instrument backgrounds; see the Experimental section) (1.36×10^6 pixels/complete image). Results from 116 similar image data sets had an average intensity S.D. of 12 % (9 and 15 % in the green and red channels respectively). In the present study, one or more of the tumour images at each time point included a part (5–10 %) of the black background adjacent to the mouse (see Figures 7B and 7D); these areas of such images served as internal controls for instrument correction and data analysis (approx. zero for both red and green channels).

	Image	Non-tumour	Control tumour (SW480*neo*)	MMP-7 tumour (SW480*mat*)	Average*
Initial	Red	62 ± 20	36 ± 10	55 ± 15	51 ± 13 (3)
	Green†	501 ± 106	513 ± 53	539 ± 67	518 ± 19 (3)
15 min	Red	69 ± 10	117 ± 26	84 ± 17	90 ± 25 (3)
	Green†	485 ± 60	576 ± 87	456 ± 73	506 ± 63 (3)
2 h	Red (A)	54 ± 11	96 ± 16	42 ± 7	48 ± 9 (2)**
	Green (A)	415 ± 47	523 ± 164	914 ± 132	
	Red (B)		87 ± 14	42 ± 7	
	Green (B)		521 ± 100	1022 ± 136	
	Green (average)	415 ± 47	522 ± 132	968 ± 134	
	Green (− non-tumour)‡	0 ± 47	107 ± 132	553 ± 134	
	Green ($n = 6$)§		101 ± 120***	668 ± 92***	

* The average values (right column) are the means ± S.E.M. from the three sets of images (non-tumour, *neo*-tumour and *mat*-tumour), except that the 2 h red-channel values (**) are the means ± S.E.M. from the non-tumour and *mat*-tumour images.

† The average green-channel fluorescence of the first two sets of measurements (initial and 15 min) is 512 ± 38 counts · (10 s)$^{-1}$ · pixel^{-1} (means ± S.E.M., $n = 6$). After approx. 24 h, the three imaged areas (non-tumour, *neo*-tumour and *mat*-tumour) gave similar fluorescence values that averaged 740 ± 84 counts · (10 s)$^{-1}$ · pixel^{-1} (means ± S.E.M.) in the green channel (results not shown).

‡ For the 2 h results, the green-channel fluorescence of the two image sets (A and B) were averaged and the amplitude above the non-specific autofluorescence/backscatter (background) was calculated by difference, taking the signal from the non-tumour area image [415 counts · (10 s)$^{-1}$ · pixel^{-1}] as background.

§ Means ± S.E.M. for the 2 h *neo*-tumour and *mat*-tumour results ($n = 6$; ***$P < 0.0001$, paired *t* test; $P = 0.028$ or 0.031 by WSR and Sign tests respectively) from similar studies of six individual mice after subtraction of the autofluorescence/backscatter backgrounds that ranged up to 2740 counts · (10 s)$^{-1}$ · pixel^{-1} (calculated from 3 s images) and averaged to 1810 counts · (10 s)$^{-1}$ · pixel^{-1}.

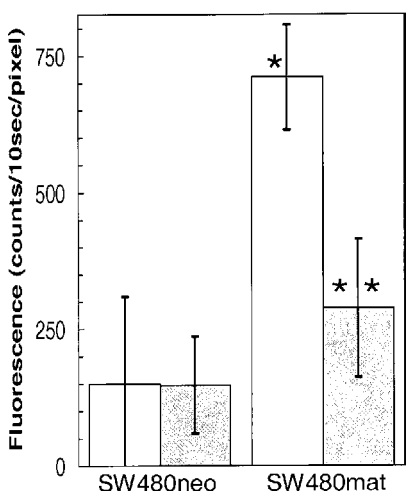

Figure 8 *In vivo* inhibition of tumour-associated MMP-7 activity by BB-94, as detected by quantitative fluorescence imaging of mouse subcutaneous xenograft tumours using PB-M7VIS

Mice bearing both SW480*neo* and SW480*mat* xenografts were each imaged as in Figure 7 (open bars), then re-imaged (shaded bars) after 2 days of treatment with BB-94 (see the Experimental section). Results are means ± S.E.M. ($n = 3$). *$P = 0.019$ (paired *t* test) and $P = 0.109$ (WSR test), comparing the fluorescence over SW480*mat* versus SW480*neo* tumours, each before BB-94 treatment (open bars). **$P = 0.056$ (paired *t* test) and $P = 0.109$ (WSR test) compared with the fluorescence over the SW480*mat* tumours before BB-94 treatment, but $P > 0.35$ (paired *t* test) and $P > 0.285$ (WSR test) compared with the fluorescence over the SW480*neo* tumours.

approx. 2.5-fold higher than the K_m value for MMP-7, may have served to enhance the *in vivo* selectivity of the reagent. Probably, it also accounts for the relatively slow generation of the tumour-associated Fl fluorescence that is not detected within the first approx. 15 min after administration of the beacon. The relatively slow appearance of signal would also suggest a relatively slow clearance of PB-M7VIS, with a pharmacokinetic profile that may be in the same range or longer than that of the parent PAMAM generation-4 dendrimer labelled with Gd that has a 35 min half-life [11]. Other yet to be defined parameters include the permeability of the beacon from the vasculature into the tumour that would also affect both the rate and extent of its activation. Approx. 2 h after administration of PB-M7VIS, the *in vivo* imaging data show enhanced Fl fluorescence associated with the MMP-7-expressing SW480*mat* tumour that is significantly above the background signal attributable to both autofluorescence and backscatter. Notably, this enhanced Fl fluorescence can be markedly diminished (to approx. 40 %) by prior systemic treatment of the animal with the MMPI BB-94. In contrast, the control SW480*neo* tumour exhibits Fl fluorescence that is only slightly above and not significantly different from the background and is unaffected by the BB-94 treatment. The simplest interpretation of these results is that the enhanced Fl fluorescence over the MMP-7-expressing SW480*mat* tumour arises from cleavage of PB-M7VIS by tumour-associated MMP-7 activity that can be, at least partially, inhibited by prior treatment of the mouse with BB-94, a broad-spectrum MMPI. After such treatment, the approx. 40 % residual fluorescence over the SW480*mat* tumour, although diminished to a level that, in the present study, is not significantly different from the control or background, may be due either to a fraction of MMP activity that is not inhibited by BB-94 using this treatment and imaging method or to other tumour-associated tissue proteinases that may be selectively induced or activated in proximity to the SW480*mat* tumours.

From a pharmacokinetic perspective for *in vivo* studies, the PAMAM dendrimer substrate described here may be comparable

with the protease-activated near-IR *in vivo* imaging probes developed by Weissleder and co-workers [7,8] that are built on a versatile methoxypoly(ethylene glycol)-protected polylysine linear co-polymer core; both types of polymer-based substrates give signal at approx. 2 h post-injection. However, PB-M7VIS differs in several respects from the protease-activated, graft co-polymer-based reagents [9,25]. The PAMAM scaffold of PB-M7VIS is available over a range of molecular masses that exhibit different rates of clearance from the circulation [11]. Such different-sized dendrimers can be utilized for specific imaging strategies, e.g. a Gd-chelate derivative of generation-8 PAMAM (233.383 kDa) has been utilized recently to visualize the mouse lymphatic system by micromagnetic resonance [26]. A particular advantage of the PAMAM core in PB-M7VIS is that its dendrimer structure facilitates flexibility in the design to optimize quenching of the fluorescence of the reagent so as to enhance the optical sensitivity of the reagent to cleavage. In PB-M7VIS, attenuation of its intrinsic fluorescence is achieved not only by introducing multiple Fls into the same polymer, resulting in homotransfer self-quenching of the 'sensor' Fls, but also by additional quenching afforded by resonance energy transfer to TMR, attached to other branches of the dendrimer. TMR fluoresces at a longer wavelength than Fl and functions as an internal reference to detect both uncleaved and cleaved reagents. Although this internal reference TMR fluorescence is useful for the *in vitro* assays to discriminate against possible non-specific proteolytic cleavage of PB-M7VIS (see Figure 4), it has particular utility for both *ex vivo* and *in vivo* protease assays. In image-based assays, the TMR internal reference provides a direct measure of the concentration of the substrate plus product although in the *in vivo* studies reported here, the concentration of PAMAM-TMR appeared to be insufficient for reproducible detection (see Table 3). The TMR internal reference of PB-M7VIS is particularly useful in *ex vivo* fluorescent microzymography studies to detect and image MMP-7 activity in frozen sections of tumours (J. O. McIntyre, B. Fingleton and L. M. Matrisian, unpublished work).

PB-M7VIS includes a peptide sequence with a relatively high affinity for MMP-7 and selectivity for this enzyme compared with MMP-2, an MMP that is frequently expressed by the stromal component of tumours. In contrast, the peptide sequence incorporated into the graft co-polymer fluorogenic reagent described by Bremer et al. [9] is a more general substrate for MMPs. That reagent selectively detected xenografts that express MMP-2 by comparison with a different type of tumour lacking MMP. The fluorescence signal was significantly attenuated by treating the animal with an MMPI, consistent with *in vivo* detection of tumour-associated MMP activity [9]. In the studies reported in the present study, both the xenografts were derived from the same SW480 human colon cancer cell line, the only difference being the expression of MMP-7 by SW480*mat* compared with the control SW480*neo* cells. The parental SW480 cells have been reported to express both MMP-9 and -14 [27] and we have confirmed that SW480*neo* and SW480*mat* cells both express equivalent levels of MMP-9 (B. Fingleton, unpublished work). After subcutaneous injection, these two cell lines develop tumours of similar mass. Histological analysis as well as MRI data indicated no significant differences in vasculature (results not shown) and, therefore, in the accessibility to reagent. Thus the SW480*neo* xenograft on the contralateral flank of the mouse serves as an appropriate control for the SW480*mat* xenograft. The results of the present study show Fl fluorescence over the SW480*neo* (control) tumour that is comparable with the autofluorescence background over a non-tumour area of the skin, with significantly enhanced Fl fluorescence only over the SW480*mat* tumour. Thus the intravenous administration of PB-M7VIS detects and images MMP-7 activity *in vivo* such that it functions as a selective PB for MMP-7 activity. For detection of signal, the activity of MMP-7 serves to light the beacon, a process that can be at least partially inhibited by prior systemic treatment of the animal with a broad-spectrum MMPI. In this context, PB-M7VIS functions as an *in vivo* optical molecular imaging contrast reagent. Reagents of this type have a potential application not only for detecting and imaging tumours via their tumour-associated MMP activity, but also for measuring the *in vivo* efficacy of MMPIs being used for therapeutic treatment of disease processes in which MMPs have been implicated, such as metastatic cancers.

We thank Kathy Carter for assistance with the animal colony. This work was partially supported by NIH [grant nos. P20 CA86283, R01 CA60867 (supplement) and P30 CA68485]. Fluorescence imaging experiments and analyses were performed in part using the VUMC Cell Imaging Shared Resource (supported by NIH grant nos. CA68485, DK20593 and DK58404). We thank Dr Charles Cobb and Dr Albert Beth (Department of Molecular Physiology and Biophysics, Vanderbilt University School of Medicine) for use of the fluorescence spectroscopy facility and the Vanderbilt-Ingram Cancer Center (partially supported by NIH grant no. P30 CA68485; Vanderbilt University Medical Center, Nashville, TN, U.S.A.) for the use of the Biostatistics Shared Resource facilities.

REFERENCES

1 Woessner, J. F. and Nagase, H. (2000) Matrix Metalloproteinases and TIMPs, Oxford University Press, New York
2 Brinckerhoff, C. E. and Matrisian, L. M. (2002) Matrix metalloproteinases: a tail of a frog that became a prince. Nat. Rev. Mol. Cell Biol. **3**, 207–214
3 Wilson, C. L. and Matrisian, L. M. (1998) Matrilysin. In Matrix Metalloproteinases (Parks, W. C. and Mecham, R. P., eds.), pp. 149–184, Academic Press, San Diego, CA
4 Newell, K. J., Witty, J. P., Rodgers, W. H. and Matrisian, L. M. (1994) Expression and localization of matrix-degrading metalloproteinases during colorectal tumorigenesis. Mol. Carcinog. **10**, 199–206
5 Wilson, C. L., Heppner, K. J., Labosky, P. A., Hogan, B. L. M. and Matrisian, L. M. (1997) Intestinal tumorigenesis is suppressed in mice lacking the metalloproteinase matrilysin. Proc. Natl. Acad. Sci. U.S.A. **94**, 1402–1407
6 Rudolph-Owen, L. A., Chan, R., Muller, W. J. and Matrisian, L. M. (1998) The matrix metalloproteinase matrilysin influences early-stage mammary tumorigenesis. Cancer Res. **58**, 5500–5506
7 Bremer, C., Ntziachristos, V. and Weissleder, R. (2003) Optical-based molecular imaging: contrast agents and potential medical applications. Eur. Radiol. **13**, 231–243
8 Weissleder, R. and Mahmood, U. (2001) Molecular imaging. Radiology **219**, 316–333
9 Bremer, C., Tung, C. H. and Weissleder, R. (2001) *In vivo* molecular target assessment of matrix metalloproteinase inhibition. Nat. Med. **7**, 743–748
10 Welch, A. R., Holman, C. M., Browner, M. F., Gehring, M. R., Kan, C. C. and Vanwart, H. E. (1995) Purification of human matrilysin produced in *Escherichia coli* and characterization using a new optimized fluorogenic peptide substrate. Arch. Biochem. Biophys. **324**, 59–64
11 Kobayashi, H., Sato, N., Hiraga, A., Saga, T., Nakamoto, Y., Ueda, H., Konishi, J., Togashi, K. and Brechbiel, M. W. (2001) 3D-micro-MR angiography of mice using macromolecular MR contrast agents with polyamidoamine dendrimer core with reference to their pharmacokinetic properties. Magn. Reson. Med. **45**, 454–460
12 Witty, J. P., McDonnell, S., Newell, K., Cannon, P., Navre, M., Tressler, R. and Matrisian, L. M. (1994) Modulation of matrilysin levels in colon carcinoma cell lines affects tumorigenicity *in vivo*. Cancer Res. **54**, 4805–4812
13 Moore, S. and Stein, W. H. (1948) Photometric ninhydrin method for use in the chromatography of amino acids. J. Biol. Chem. **176**, 367–388
14 Moore, S. (1968) Amino acid analysis: aqueous dimethyl sulfoxide as solvent for the ninhydrin reaction. J. Biol. Chem. **243**, 6281–6283
15 Whittaker, M., Floyd, C. D., Brown, P. and Gearing, A. J. H. (1999) Design and therapeutic application of matrix metalloproteinase inhibitors. Chem. Rev. **99**, 2735–2776
16 Segel, I. H. (1975) Enzyme Kinetics, John Wiley and Sons, New York
17 Netzel-Arnett, S., Sang, Q. X., Moore, W. G., Navre, M., Birkedal-Hansen, H. and Van Wart, H. E. (1993) Comparative sequence specificities of human 72- and 92-kDa gelatinases (type IV collagenases) and PUMP (matrilysin). Biochemistry **32**, 6427–6432
18 Vargas, G., Chan, K. F., Thomsen, S. L. and Welch, A. J. (2001) Use of osmotically active agents to alter optical properties of tissue: effects on the detected fluorescence signal measured through skin. Lasers Surg. Med. **29**, 213–220
19 Smith, M. M., Shi, L. and Navre, M. (1995) Rapid identification of highly active and selective substrates for stromelysin and matrilysin using bacteriophage peptide display libraries. J. Biol. Chem. **270**, 6440–6449

20 Kridel, S. J., Sawai, H., Ratnikov, B. I., Chen, E. I., Li, W., Godzik, A., Strongin, A. Y. and Smith, J. W. (2002) A unique substrate binding mode discriminates membrane type-1 matrix metalloproteinase from other matrix metalloproteinases. J. Biol. Chem. **277**, 23788–23793
21 Chen, E. I., Kridel, S. J., Howard, E. W., Li, W., Godzik, A. and Smith, J. W. (2002) A unique substrate recognition profile for matrix metalloproteinase-2. J. Biol. Chem. **277**, 4485–4491
22 Yoo, H. and Juliano, R. L. (2000) Enhanced delivery of antisense oligonucleotides with fluorophore-conjugated PAMAM dendrimers. Nucleic Acids Res. **28**, 4225–4231
23 McCawley, L. J. and Matrisian, L. M. (2001) Matrix metalloproteinases: they're not just for matrix anymore! Curr. Opin. Cell Biol. **13**, 534–540
24 Diehl, K.-H., Hull, R., Morton, D., Pfister, R., Rabemampianina, Y. and Smith, D. (2001) A good practice guide to the administration of substances and removal of blood, including routes and volumes. J. Appl. Toxicol. **21**, 15–23
25 Mahmood, U., Tung, C. H., Bogdanov, Jr, A. and Weissleder, R. (1999) Near-infrared optical imaging of protease activity for tumor detection. Radiology **213**, 866–870
26 Kobayashi, H., Kawamoto, S., Star, R. A., Waldmann, T. A., Tagaya, Y. and Brechbiel, M. W. (2003) Micro-magnetic resonance lymphangiography in mice using a novel dendrimer-based magnetic resonance imaging contrast agent. Cancer Res. **63**, 271–276
27 Giambernardi, T. A., Grant, G. M., Taylor, G. P., Hay, R. J., Maher, V. M., McCormick, J. J. and Klebe, R. J. (1998) Overview of matrix metalloproteinase expression in cultured human cells. Matrix Biol. **16**, 483–496

Received 17 April 2003/10 October 2003; accepted 14 October 2003
Published as BJ Immediate Publication 14 October 2003, DOI 10.1042/BJ20030582